ACS Sustainable Chemistry & Engineering

pubs.acs.org/journal/ascecg

Research Article

Isopropanol Mediates the Rapid and Selective Synthesis of Vaterite during Ambient Carbonation

Jenny Arabit, Dale Prentice, Justin Luong, Arnaud Bouissonnié, Jagannathan Govindhakannan, Fabian Rosner, Dante Simonetti, Erika La Plante, Torben Gadt, and Gaurav Sant*

Cite This: *ACS Sustainable Chem. Eng.* 2025, 13, 7549−7561

Read Online

ACCESS | Metrics & More | Article Recommendations | Supporting Information

ABSTRACT: Vaterite is a metastable polymorph of calcium carbonate ($CaCO_3$) that can be controllably transformed into aragonite or calcite (i.e., stable $CaCO_3$ polymorphs) − via a dissolution−precipitation pathway − thereby enabling cementation. Despite its potential as a low-carbon cementitious material, vaterite's synthesis and stabilization at high yield, particularly when using alkaline calcium solids and gas-phase carbon dioxide (CO_2) as reactants, remain a challenge. Here, for the first time, we demonstrate that isopropanol (IPA) enables the direct utilization of a dilute gas-phase CO_2 (∼5 vol %) stream to rapidly and controllably synthesize vaterite using technical hydrated lime (portlandite: $Ca(OH)_2$) as a Ca-source at ambient temperature and pressure. It appears that, in aqueous solution and in the presence of monohydric alcohols, a surface tension less than 30 mN/m and a viscosity greater than 2 mPa·s promote the selective precipitation of vaterite. But, this suggestion was unfounded as these solution properties alone do not explain the exceptional vaterite selectivity (>80 mass %) that was achieved only in IPA-water mixtures. The findings indicate a pioneering approach for the use of IPA to mediate the continuous synthesis of vaterite using technical reagents (hydrated lime and CO_2) with implications for cement decarbonization, and CO_2 mineralization and utilization.

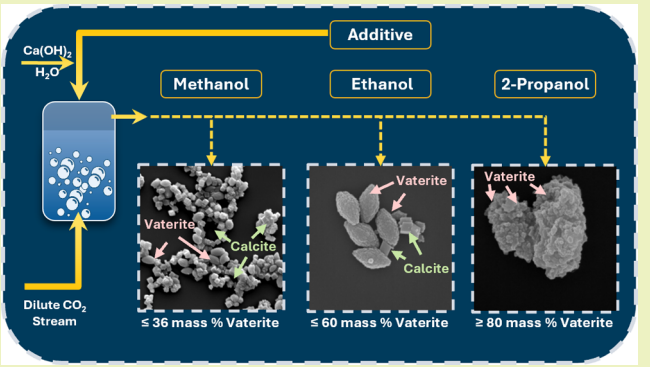

KEYWORDS: *calcium carbonate, cement, vaterite, ambient carbonation, CCUS*

INTRODUCTION AND BACKGROUND

Concrete, a mixture of cement (Ordinary Portland Cement, OPC), sand, stone, and water, forms the basis of our built environment. While the role of concrete as the most prevalent construction material is unarguable, the production of cement—the binding agent in concrete, is associated with an enormous carbon footprint.[1] Today, the production of ∼4.5 billion tonnes of cement annually accounts for nearly 10% of global carbon dioxide (CO_2) emissions.[2] To address cement's enormous CO_2 footprint, there is increasing interest in approaches including CCUS (carbon capture, utilization, storage), and the development of nonsilicate cement chemistries. Inspired by both considerations, i.e., to enable CO_2 utilization, and to (re)create nature's own structural cementation solution, i.e., calcium carbonate that makes up the exoskeleton of numerous marine organisms, this work develops new approaches for the selective and continuous synthesis of vaterite. The nonclassical nucleation of calcium carbonate ($CaCO_3$) in aqueous solution follows a thermodynamic "downhill" cascade that initiates with the formation of prenucleation clusters (PNCs), which aggregate in due course to form, in order of stability: amorphous calcium carbonate (ACC), vaterite, aragonite, and calcite.[3−5] The latter constituents represent crystalline compounds, of which vaterite, like ACC, is metastable, i.e., it has a tendency to transform into (generally) calcite.[6] Thus, the production of vaterite requires a means to controllably arrest the downhill cascade such that once formed, vaterite will persist, and not transform via a dissolution-(re)precipitation process into calcite.

Over the past decade, there has been growing interest in the general area of CO_2 utilization. Herein, it is sought to carbonate alkaline solids, in the presence of water, by direct (e.g., exposure to gas-phase CO_2 of preformed, or fresh concrete), or indirect (e.g., exposure to dissolved soluble carbonates) methods.[7,8] The concentration of the CO_2 feedstock (e.g., gas-phase, or dissolved species) and the carbonation conditions (e.g., ambient (p,T) or superambient conditions such as elevated temperature, and pressure)

Received: February 19, 2025
Revised: May 9, 2025
Accepted: May 12, 2025
Published: May 16, 2025

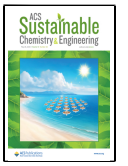

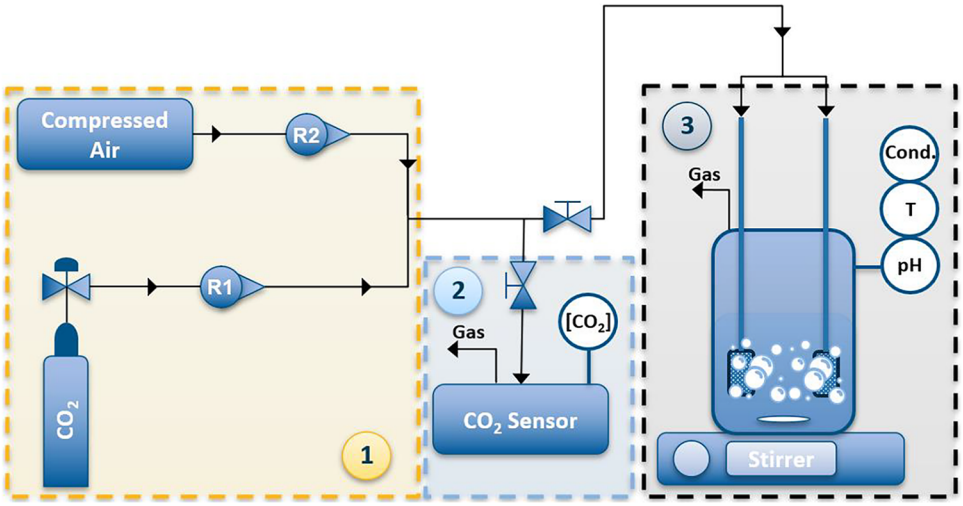

Figure 1. Experimental setup consisting of: (1) a gas feed preparation section, (2) a vessel to measure the $[CO_2]$ of the inlet gas stream, and (3) a carbonation reactor.

determine the rate of carbonation. In the vast majority of these cases, no attempt is made to control the nature of the calcium carbonate reaction product, although depending on the reaction conditions different polymorphs may be observed.[8] Recently, there has been interest in the use of vaterite as a cementing agent. In particular, Hargis et al. have definitively shown the ability to exploit the polymorphic (thermodynamic) transition from vaterite to aragonite (and calcite) to produce carbonate-bonded composites which show compressive strengths up to 40 MPa (N.B.: ∼90% of all concrete produced globally features compressive strengths inferior to 40 MPa).[9,10] While others have shown similar results, for the most part, the scalable production of vaterite, industrially, remains a challenge. The one standout example in this regard is the work of Fortera (Hargis et al., whose lineage derives from Calera Inc.), which is currently commercializing a proprietary vaterite-based OPC-clinker extension solution, i.e., whereby vaterite is used to partially replace cement in the binder fraction of concrete.

Vaterite presents distinguishing attributes vis-à-vis the other $CaCO_3$ polymorphs including: (i) enhanced flowability on account of its spherical/raspberry-like morphology,[11] (ii) greater reactivity on account of its higher solubility (e.g., vaterite is ∼3.7 times more soluble than calcite and ∼2.5 times more soluble than aragonite), and (iii) high specific surface area because vaterite particles consist of agglomerates of submicron vaterite building blocks.[12,13] These attributes are desirable not only for controlling cementation behavior, but make vaterite desirable in other applications including: as a substrate for API (active pharmaceutical ingredient) attachment in pharmaceutical applications, as a mineral filler in polymer sealants, and for use as a catalyst substrate, etc.[14,15] In the context of CO_2 utilization, the production of vaterite, if accomplished using $Ca(OH)_2$ ("CH") could uptake ∼0.59 g of CO_2 per g of CH. While this is most desirable when coupled with a method for making zero-carbon lime (e.g., via the ZeroCAL process), this approach is attractive since it may be amenable to the use of dilute CO_2 sources (i.e., ∼3-to-30 vol % CO_2), thereby allowing direct utilization of CO_2 containing industrial flue gas streams, without a need for a carbon capture (i.e., "concentration increase") step.[16,17]

The most well-developed method for industrial vaterite production utilizes ammonium salts (e.g., NH_4OH and NH_4NO_3).[10,18] In this case, ammonium (NH_4^+) stabilizes the (001) hexagonal face to precipitate and stabilize vaterite in solution.[19] Hargis et al. demonstrated the scalability of this method by carbonating a carbide lime and NH_4Cl mixture with a gas stream containing 11 vol % CO_2.[10] In this process, NH_4OH is often formed during the solubilization of the alkaline calcium feedstocks (e.g., $Ca(OH)_2$, CaO, slag, etc.), wherein NH_4Cl is used to increase the aqueous concentration of Ca^{2+}.[10,20,21] The complexity with using ammonium salts stems from the thermal sensitivity of NH_4OH, which is necessary for enhancing CO_2 absorption during carbonation. The sensitivity of NH_4OH to temperature stems from its low boiling point of 38 °C (at 25 mass % NH_3). This thermal sensitivity requires strict control of reaction temperature to maintain the operating pH and additive concentration and vaterite selectivity. The difficulty of controlling the process temperature becomes more challenging with increasing production scale on account of the heat evolved during solubilization and subsequent carbonation.[20,22]

To overcome these challenges, this study demonstrates a unique method to produce vaterite (≥80 mass % selectivity vis-à-vis calcite) using solid $Ca(OH)_2$ (i.e., in lieu of predissolved ionic precursors) and a dilute CO_2 gas stream (5 vol % CO_2) at ambient conditions (i.e., $T \sim 25$ °C and p = 1 atm). The approach ensures vaterite's formation in the presence of water-miscible hydroxylated additives (e.g., saccharides and alcohols).[23−26] The hydroxyl groups of these additives are hypothesized to affect the activity of water and ions in the crystallization domain.[27−30] By doing so, the additives may not only influence the $CaCO_3$ crystallization pathway in favor of a downhill energetic sequence that begins with the formation of an ACC precursor but also impedes the dissolution-(re) crystallization mechanism that otherwise transforms vaterite into the more stable $CaCO_3$ polymorphs (i.e., aragonite and calcite).[6,31] The efficacy of using these additives in controlling $CaCO_3$ polymorphism even with gas phase CO_2 has been demonstrated by previous authors.[25,26,32] However, these studies often use pure CO_2 gas streams, which may restrict their potential by obviating the direct utilization of dilute CO_2 streams (≤30 vol % CO_2).[17] To this end, five

https://doi.org/10.1021/acssuschemeng.5c01554
ACS Sustainable Chem. Eng. 2025, 13, 7549−7561

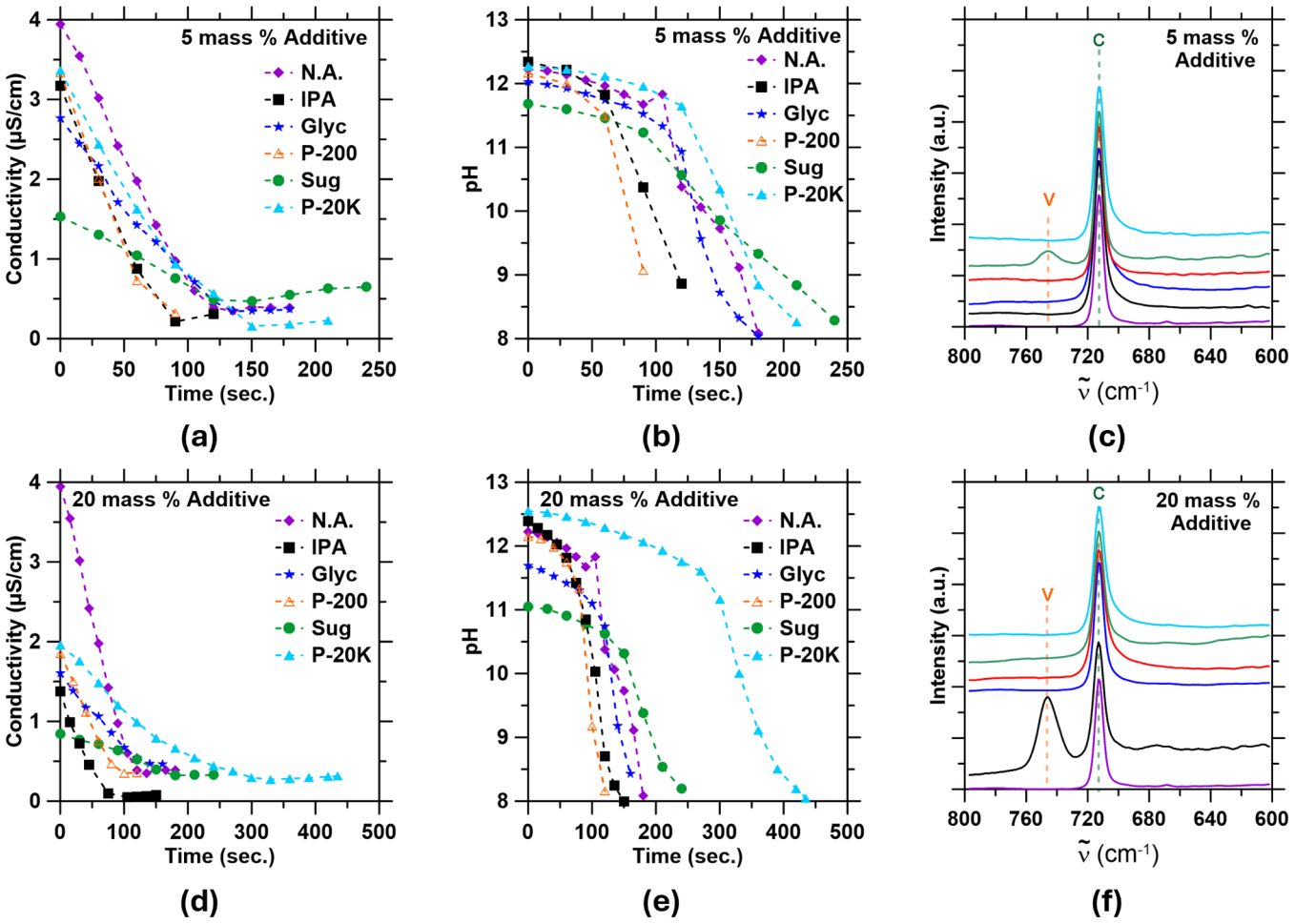

Figure 2. (**Top**) Representative traces of the (a) solution conductivity and (b) pH during carbonation of a solution containing 5 mass % additive. (**Bottom**) The corresponding time-dependent evolution of the (d) solution conductivity and (e) pH for solutions with 20 mass % additive. The IR spectra of the carbonate precipitates from solutions with (c) 5 and (f) 20 mass % additive. The characteristic peaks for vaterite ("V") and calcite ("C") are indicated. The curves labeled "N.A." refers to carbonation carried out without any additive in solution, while "P-200" and "P-20K" refer to PEG − 200 and PEG − 20000, respectively.

(potential) vaterite formers were considered: 2-propanol (IPA), glycerol, polyethylene glycol (PEG) 200, sucrose, and PEG − 20,000. The incorporation of each additive into the reaction solution at 5 and 20 mass % additive was found to affect the characteristics of the solution and, consequently, $CaCO_3$ precipitation. Given the hypothesized role of mass transport and solution thermodynamics on $CaCO_3$ transformation, the influence of the solution's viscosity (η), surface tension (σ), and thermodynamic activity of water (a_w) on vaterite precipitation were examined in the presence of methanol (MeOH), ethanol (EtOH), n-propanol (n-Pr), 2-propanol (IPA), and *tert*-butyl alcohol (tBA).

MATERIALS AND METHODS

Experimental Details. Carbonation was carried out in semibatch mode using a 500 mL baffled glass reactor (Wilmad Glass LG − 8079B) under constant stirring (700 rpm, see Figure 1). The inlet gas stream was split between two sintered ceramic gas spargers (ø = 3 cm) that were placed at opposite ends of the reactor's diameter. Two electrodes that measure pH (Thermo Scientific 8302BNUMD) and conductivity (Thermo Scientific 013005MD) were inserted into the solution to monitor the pH and ionic conductivity during carbonation. A 200 g mixture containing ∼10 mmol CH/kg of solution and a prescribed mass of a given additive (as summarized in Tables S2 and S3) was prepared for each experiment. For the PEG-20000, a portion of the water was used to dissolve the solid reactant. The amount of water partitioned was determined based on the minimum amount required to fully dissolve the mass of $Ca(OH)_2$ (i.e., ∼20 mmol/L of water at 25 °C). The reported additive mass fractions (m_i) were calculated using the mass of the additive and water due to the relatively low mass/solubility of added $Ca(OH)_2$. The water activity (a_w) of the solution mixtures noted in Tables S2 and S3 was either retrieved from the literature or calculated using Van Laars equations and a modified Raoult's law (see eqs S1−S4 and Table S4 under the Experimental Details section in the Supporting Information). Additionally, the surface tension (σ) and viscosity (η) of the monohydric solutions were retrieved from literature and are summarized in Table S3.

An air/CO_2 gas mixture consisting of 5 ± 1 vol % CO_2 was composed by mixing air with CO_2 (Medical USP; >99 vol % purity). Two mass flow controllers (Brooks Instruments: Sho-rate) regulated the air and CO_2 flow rates to produce the desired gas mixture with a total flow rate of 1500 standard cubic centimeters (see Section 1 in Figure 1). This gas mixture was fed into a separate vessel housing the CO_2 sensor (Dracal: DXC220; Section 2 in Figure 1) to equilibrate to the target CO_2 concentration. Representative curves of the gas stream [CO_2] (vol %) and the respective average [CO_2] are shown in the Supporting Information (see Figure S2(a,b)). Thereafter, the gas mixture was fed into a carbonation reactor (Section 3 in Figure 1), wherein the reaction was terminated when the solution pH decayed from >11.5 to ∼ 8. Thereafter, the solution was vacuum filtered

https://doi.org/10.1021/acssuschemeng.5c01554
ACS Sustainable Chem. Eng. 2025, 13, 7549−7561

through a 0.22 μm PTFE membrane filter. The filtered precipitates were rinsed with ethanol twice and oven-dried at 50 °C for 1 h.

Materials. Calcium hydroxide ($d_{50} \sim 3$ μm, ≥89 mass % purity), CO_2 (>99 vol % purity), and distilled water were used. Reagent grade methanol (≥99.8% purity), ethanol (≥99.2 mass % purity), n-propanol (≥99.5 mass % purity), 2-propanol (≥99.5 mass % purity), tert-butanol (≥95 mass % purity), glycerol (≥99.5 mass % purity), sucrose (≥99 mass % purity), polyethylene glycol 200 (≥95 mass % purity), and polyethylene glycol 20000 (≥95 mass % purity) were purchased from Fisher Scientific and used as received. It is important here to note that all the additives only serve as reaction mediators, i.e., while they may affect or facilitate $CaCO_3$ precipitation, they are not consumed over the course of reactions.[30,33]

Material Characterization. First, Attenuated Total Reflectance Fourier Transform Infrared Spectroscopy (ATR-FTIR: Spectrum Two FT-IR Spectrometer, PerkinElmer) was used to identify the carbonate polymorphs in the precipitates following carbonation. Using this technique, the collected solids (i.e., prior to oven drying) can be characterized with minimal sample preparation and delay. After filtration, the solids were loaded onto a diamond/ZnSe composite crystal and the absorption spectra over the range of 450−4000 cm^{-1} were collected. The $CaCO_3$ polymorphs were identified using their characteristic peaks, signifying symmetric stretching (ν_1), out-of-plane bending (ν_2), in-plane asymmetric stretching (ν_3), and in-plane bending (ν_4) of the carbonate groups (see Table S1). Due to the large overlap of the absorption bands, the ν_4 vibrational modes (i.e., characteristic peaks within 700−800 cm^{-1}) were used as unique identifiers for the anhydrous polymorphs, whereas the ν_2 vibrational mode was used to discern amorphous calcium carbonate (ACC).[34−37] $Ca(OH)_2$ (portlandite) was identified using the ∼3640 cm^{-1} peak of the O−H stretching vibration.

Second, the particulates were characterized using X-ray powder diffraction (XRD: Panalytical X'Pert Pro X-ray Powder Diffractometer) using Cu−Kα radiation (1.5410 Å). The dried samples were loaded onto a zero-background plate (Si-sample holder) and analyzed at a scan rate of 38.7350 s/step and a 0.0170° (2θ) step size over a 2θ range of 5−70°. Quantitative "Rietveld" refinement of the X-ray reflections (QXRD) was performed using Profex.[38] The following mineral phases were identified: portlandite (PDF #04-010-3117), calcite (PDF #04-008-0788), and vaterite (COD #9015898), when present.[39] Third, the QXRD results were compared with the thermogravimetric analysis (TGA: STA 8000, PerkinElmer) results. Around 20 mg of dry powder was placed in a pure aluminum oxide crucible and heated at a temperature ramp rate of 15 °C/min over a temperature range of 35−975 °C. The analysis was carried out using ultrahigh-purity N_2 as a purge gas at 20 mL/min. The mass loss below 200 °C was attributed to the evaporation of water, while the mass loss over the temperature range of 360−550 °C and 550−900 °C was associated with the decomposition of $Ca(OH)_2$ and $CaCO_3$, respectively (as shown in Figure S1(a)).[40] Thermal analysis of the hydrated lime reactant indicated an impurity of about 5 mass % $CaCO_3$ that was identified as calcite by XRD (see Figure S1(b)).

Finally, the precipitate morphology was assessed using scanning electron microscopy (SEM: FEI Nova 230). To prepare the sample for SEM imaging, the dried particulates were suspended in 2-propanol and sonicated to break apart large aggregates that were formed during drying and storage. An aliquot (<200 μL) of this suspension was then drop-casted on to a Si-wafer substrate and gold-coated after vacuum drying overnight. Imaging was carried out using an Everhart-Thornley detector (ETD) and a through-the-lens detector (TLD) at high vacuum at an accelerating voltage of 10 kV and a working distance of ∼5 mm. A TLD was used to achieve greater magnifications and capture high-resolution images of the submicron to micron-sized particulates.

RESULTS AND DISCUSSION

The Influence of Additives on $CaCO_3$ Polymorphic Selectivity. Foremost, an experimental control was established by the carbonation of a neat $Ca(OH)_2$ ("CH") solution. The results were compared with thermodynamic simulations (see: Figure S3 under the Thermodynamic Modeling section in the Supporting Information) to relate *in situ* measurements of pH and conductivity to the chemical speciation during carbonation. To establish a common link between the simulation and experimental results, the elapsed time was converted to the cumulative moles of CO_2 input, as shown in Figure S3. Upon introducing CO_2, an immediate reduction in the solution conductivity and a slight reduction in pH were observed (see Figure 2). These trends align with the thermodynamic simulations that show a rapid decline in ionic strength (i.e., due to precipitation) and a smaller change in the pH (see Figure S3(a-b)) once CO_2 was added. Despite the small change in pH, Figure S3(a) shows a continuous increase in $CaCO_3$ content, indicating that the observed decline in the solution's conductivity was caused by the rapid consumption of mobile ions (i.e., $Ca^{2+}$and OH^-) and precipitation of $CaCO_3$ according to eq 1.

$$Ca(OH)_2 + CO_2 \rightarrow CaCO_3 + H_2O \quad (1)$$

A continuous reduction in the ionic strength and conductivity occurs until ∼ 10 mmol/L of CO_2 addition, i.e., which corresponds with the initial 10 mmol/L of $Ca(OH)_2$ feedstock. The continued decline of the ionic strength and the absence of charged carbonate species below 10 mmol/L of added CO_2 indicate its mineralization in the form of $CaCO_3$ until the system is depleted of Ca^{2+}. Thereafter, additional CO_2 introduced accumulates in the form of dissolved inorganic carbon (DIC) species according to eqs 2−4 as shown in Figure S3(c). This speciation is accompanied by proton (H_3O^+) generation that reduces the solution pH and marginally increases the ionic strength. CO_2 solvation proceeds until the solution reaches saturation (i.e., equilibrium) at ∼15 mmol/L of CO_2 addition. Any further additions beyond this point result in the degassing of CO_2 as shown in Figure S3(c).

$$CO_2 + H_2O \rightarrow H_2CO_3 \quad (2)$$

$$H_2CO_3 + OH^- \rightarrow HCO_3^- + H_2O \quad (3)$$

$$HCO_3^- + H_2O \rightarrow CO_3^{2-} + H_3O^+ \quad (4)$$

The excellent agreement between the experiments and thermodynamic simulations confirms that a terminal pH of 8 signals the maximum extent of $CaCO_3$ precipitation. Any additional CO_2 that is introduced after this point would be present as DIC species (see Figure S3(c)), which may promote the transformation of vaterite into aragonite or calcite. Unsurprisingly, without any additives (denoted as "N.A.") present, calcite is the exclusive reaction product as shown in Figure 2(c).[41−43] Previous authors have often attributed this to the thermodynamically limited absorption of CO_2 (i.e., dependence on p_{CO2} and temperature) and the uniformity of its dispersion in bulk solution.[8] With an air/CO_2 gas mixture containing 5 vol % CO_2 (i.e., p_{CO2} = 0.05 atm or ∼50,000 ppm of CO_2), the rapid mineralization of CO_2 (compared to its slower absorption, speciation and transport: see eqs 2−4) may produce a reaction front with a high concentration of DIC species − at the point of CO_2 addition − and a depleted bulk volume solution. Consequently, near the gas sparger, the high reactant concentration favors $CaCO_3$ nucleation, which is hypothesized to be conducive to vaterite precipitation.[8] However, as the metastable $CaCO_3$ diffuses away from the gas source, the reduction in calcium and carbonate

https://doi.org/10.1021/acssuschemeng.5c01554
ACS Sustainable Chem. Eng. 2025, 13, 7549−7561

concentrations (i.e., the decrease in the saturation index, SI, unitless) along with the increased contact with water promotes the transformation of more soluble vaterite into calcite.[44] This renders the system supersaturated with respect to calcite, thereby favoring further calcite formation while curtailing vaterite precipitation. Hence, additives are necessary to selectively precipitate and stabilize vaterite when it is precipitated in solution.[8]

A key challenge with the additive choice is the uncertainty in the exact mechanism that results in the selective precipitation of vaterite. The chosen array of additives in this study is thought to favor the formation of vaterite by regulating the activity of solvated Ca^{2+} and CO_3^{2-} species. Such interactions may be achieved through: (i) electrostatic interactions between an additive and a Ca^{2+} cation or CO_3^{2-} anion, and/or (ii) controlling the polarizability and hydrogen bonding interactions of and with water. The former refers to additive − Ca^{2+} (CO_3^{2-} or HCO_3^-) coordination to influence the nucleation pathway of $CaCO_3$, which may be accomplished using either ionic or nonionic additives.[30,45] For nonionic additives, the preferential solvation of Ca^{2+} or CO_3^{2-} alters the solvation shell composition around each ion and, consequently, the associated energy for ion dehydration, and subsequently, the crystallization pathway of $CaCO_3$.[46] Some authors postulate that these interactions influence the resulting structure of the so-called prenucleation clusters (PNC), whose *imprint* indicates the $CaCO_3$ polymorph that will mature/stabilize/persist over the course of crystallization.[3,4] Upon precipitation of the metastable phases, face-specific adsorption of the additive on evolving $CaCO_3$ surfaces can further assist with stabilization. Another method to promote the formation of metastable phases in solution is by leveraging the extent of hydrogen bonding between water and the additive to reduce the rate of $CaCO_3$ transformation, i.e., restrict $CaCO_3$ and water activity to kinetically inhibit the dissolution and transformation of vaterite.[6]

These interactions can be observed with sucrose ("Sug"; pK_a = 12.35) and glycerol ("Glyc"; pK_a = 13.70) in solution.[47] Introduction of these additives into the alkaline CH solution (pH ∼ 12.2) is accompanied by a slight reduction of the solution pH (see Figure 2(b),2(e)) due to the partial deprotonation of the additive and the formation of solvated species (i.e., sucrose to sucrate and glycerol to glycerolate).[26,47,48] The hydroxyl dense anions that are formed strongly interact with CO_2, Ca^{2+}, and the surrounding water to influence the crystallization of $CaCO_3$. For instance, these anions catalyze CO_2 absorption to increase the local saturation index (SI, unitless. For $CaCO_3$, SI = $\log_{10}[(\{Ca^{2+}\}\{CO_3^{2-}\})/K_{SP}]$, where { } indicates ion activities, and K_{SP} is the solubility product).[47] In addition, these anions simultaneously interact with Ca^{2+} and the surrounding water, which shifts the driving force of the reaction (i.e., from thermodynamic to kinetic) in favor of metastable phases.[6] As such, among the additive array, sucrose was expected to favor vaterite formation (see Figure 2(c)) on account of its greater anion speciation (see Table S5 under the Thermodynamic calculations section in the Supporting Information) and hydroxyl density. With seven hydroxyls per molecule, sucrate anions can greatly suppress the activity of the surrounding water, which, in turn, can affect the structure of ACC and the stability of metastable phases, including ACC and vaterite.[26] The marked ability of sucrose in stabilizing metastable phases even at dilute CO_2 concentrations (5 vol %), is exemplified by the observed precipitation of vaterite in a 5 mass % sucrose solution (see Figure 2(c)). In general, the precipitation of vaterite was observed within 1 min of carbonation and persisted even after 30 min of continuous carbonation (see Figure S4(c)). Although calcite remained the major reaction product, Kim et al. demonstrated that the reaction can be switched to vaterite-dominant (>90 mass %) with a concentrated CO_2 gas stream,[26] which increases the aqueous CO_2 concentration by 95% (e.g., per Henry's law $[CO_2]_{aq.} = p_{co2}/K_H$, where p_{co2} and K_H denotes the partial pressure of CO_2 and Henry's Law constant which takes a value of 34 mmol/L atm at 25 °C, respectively).

In spite of the promising observation of vaterite formation in the 5 mass % sucrose solution, a further increase in sucrose concentration did not enhance vaterite formation (see Figure 2(f)). Surprisingly, Kim et al. noted a reduction in vaterite selectivity when sucrose was added at a dosage that resulted in a stoichiometric excess with respect to Ca^{2+}.[26] Interestingly, an analysis of sucrate speciation revealed that while the sucrate concentration in 5 mass % sucrose (34 mM sucrate) was comparable to the 20 mass % sucrose (39 mM sucrate), the "free sucrose" concentration increased by nearly 6x (see Table S5) at the higher dosage. The slightly higher sucrate concentration indicates greater acidification of the solution and a lower initial pH (see Figure 2(e)), which influences DIC speciation and the overall SI. In addition, a greater concentration of hydroxyl-dense sucrose (i.e., eight hydroxyls per sucrose molecule) enhances hydrogen bonding (i.e., sucrose − sucrose and sucrose − H_2O) in the solution, which leads to an increase in solution viscosity. These results, in conjunction with the findings reported by Kim et al., suggest that more than the sucrose speciation, the carbonate speciation, and the effects of solution hydrodynamics (i.e., surface tension, viscosity) may be more relevant.[26]

The greater importance of the solution's hydrodynamics − on reaction dynamics − is substantiated by the observed precipitation of vaterite in 20 mass % IPA and the exclusive formation of calcite in PEG solutions (see Figure 2(f)). In contrast to sucrose and glycerol, IPA and the PEG additives maintain their protonated forms in solution (e.g., as evidenced by the unaltered initial pH in Figure 2(b),2(e)). As such, these additives influence $CaCO_3$ crystallization through weaker dipole interactions with Ca^{2+} and hydrogen bonding with water.[49,50] The larger molecular structure and negatively charged backbone of the PEG additives enhances interactions with water molecules resulting in a greater increase in solution viscosity (e.g., a 4.5× and more than 25× increase with 5 and 20 mass % of PEG 20,000, respectively).[51] Some studies have suggested that viscous solutions promote the formation of metastable phases due to the reduced ion and water activities that are prevalent in these systems.[6] This may suggest that a well-mixed viscous solution with a sufficiently high initial SI may favor ACC formation and prevent vaterite dissolution by bypassing the traditional ion−ion attachment pathway that is endemic to classical nucleation processes. In particular, the favorable increase in vaterite selectivity in a 20 mass % IPA solution suggests synergistic effect related to an increase in viscosity (η; 1.54× increase for 20 mass % IPA), and reduction in surface tension (σ; 0.57× decrease for 20 mass %), and water activity (a_w), that are consequent with increasing additive dosage.

To gain quantitative insight into the reaction kinetics, a zeroth-order rate constant (k) describing the rate of hydroxyl consumption (see eqs 5−6) was derived from the change in

https://doi.org/10.1021/acssuschemeng.5c01554
ACS Sustainable Chem. Eng. 2025, 13, 7549−7561

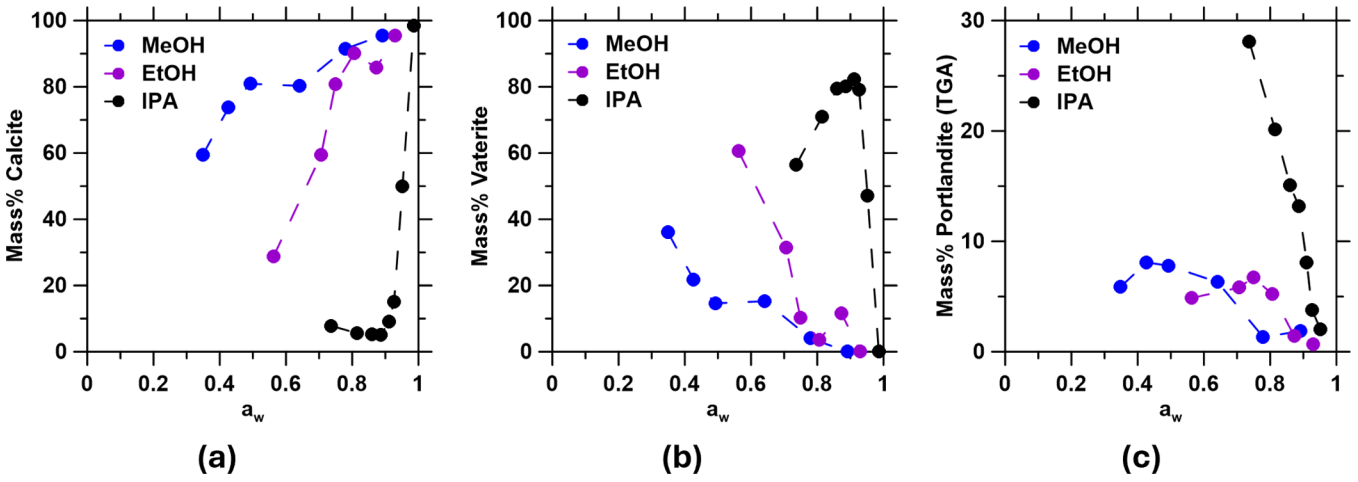

Figure 3. Mass composition of (a) calcite and (b) vaterite in the carbonated particulate product as a function of a_w for each alcohol based on QXRD results (see Supporting Information: Table S7). Also shown is the mass % of (c) unreacted portlandite based on thermogravimetric analysis (TGA). As a point of reference, at t = 0 s, the portlandite purity of the reactant is 89.8−95 mass % (see Figure S1(a)).

pH during carbonation. The rate order was identified using the integral method for a batch system as detailed under the $CaCO_3$ Precipitation: Extracting Rate Constants section in the Supporting Information. For example, Figure S5 shows that the data sets for 5 and 20 mass % additive were best captured by the zeroth-order rate law, indicating a concentration-independent rate constant, as additionally affirmed by the fixed instantaneous rate of $[OH^-]$ consumption irrespective of $[OH^-]$ concentration in Figure S6. This indicates that "k" represents the general influence of a given additive on the rate of acidification of the solution, whether it may be due to mass transport or reaction-limited kinetics

$$\frac{d([OH^-])}{dt} = -kt \tag{5}$$

$$[OH^-] = [OH^-]_{t=0} - kt \tag{6}$$

Table S6 shows that the rate constants decreased in the order: IPA > PEG-200 > N.A. ≈ PEG-20,000, which does not follow the scaling of the solution viscosities, which decreased in the order: PEG-20,000 > PEG-200 > IPA > N.A.. First, this indicates that the solution viscosity alone is not the dominant variable that affects the reaction rates. In particular, with 5 mass % additive, the rate constants of the IPA and PEG − 200 systems were found to be 1.75× and 1.48× of the control. However, with 20 mass % additive, a further increase was observed with IPA (2.13x of the control) while PEG − 200 showed a slight decrease (1.19× of the control). This kinetic enhancement is ascribed to the disruption of the hydrogen bonding environment between water molecules by $-CH_3$ dense molecules like IPA and PEG − 200 that additionally accumulate at the liquid−vapor interface. The accumulation at the liquid−vapor interface leads to significant reductions in the surface tension. For instance, a 20 mass % replacement of water with IPA or PEG − 200 results in a 57% or 20% reduction in surface tension, respectively.[52,53] This reduction in surface tension enhances CO_2 absorption and the resulting SI, which may favor vaterite formation. Additionally, assuming that precipitation initiates at the liquid − vapor interface, this allows the aggregated IPA molecules on the interface to restrict water activity in the vicinity of the precipitating vaterite. This suggests a pathway to exert "polymorphic control" of $CaCO_3$ by affecting the water activity (a_w), viscosity (η), and surface tension (σ). To assess these effects, alcohol−H_2O solutions (i.e., methanol (MeOH), ethanol (EtOH), and IPA) containing 20-to-90 mass % of an alcohol were prepared as summarized in Table S3. Similar to IPA, methanol (MeOH) and ethanol (EtOH) are short-chain monohydric alcohols that can easily intercalate between water molecules to reduce the surface tension (σ) while only marginally increasing the viscosity (η) of the alcohol−water mixture (see Table S3). The incorporation of these additives influences the activity of chemical species (i.e., Ca^{2+}, H_2O, CO_2 (aq.), and $CaCO_3$) and the resulting reactant transport and bubble dynamics in the reactor volume (i.e., bubble size and morphology, and gas permeation).[54−56]

Influence of Thermodynamic Activity of Water (a_w). Water is thought to direct the crystallization pathway of ACC and facilitate the polymorphic transformation of $CaCO_3$ via dissolution-reprecipitation processes.[6] Thus, a greater a_w was hypothesized to favor calcite precipitation in two possible ways: by promoting the dissolution of more soluble vaterite (vis-à-vis calcite) or by increasing the amount of water incorporated into ACC's evolving structure, which is thought to favor its transformation into calcite.[6,57] Using alcohol−H_2O solutions, a range of water activities, i.e., 0.25 < a_w < 1.00 (unitless), were investigated. The proposed relationship between a_w and calcite formation is shown in Figure 3(a). In general, a higher calcite content implies a lower vaterite content, and calcite is dominant for a_w > 0.90 across the three alcohol systems, as shown in Figure 3(b). On the other hand, the observed reduction in vaterite content in the IPA solutions for a_w < 0.90 is related to the reduction in $Ca(OH)_2$ conversion, which implicates a reduced CH dissolution in this system, as shown in Figure 3(c), and as indicated by the low(er) calcite content seen in Figure 3(a).

Interestingly, a greater extent of water replacement with alcohol (i.e., decreasing a_w) was also found to stabilize ACC as qualitatively shown by the gradual peak broadening in the diffraction and IR spectra (see Figures S7 and S8, respectively). This lower degree of crystallinity at higher alcohol concentrations is corroborated by the corresponding TGA data of the dried particulates. In particular, the precipitates of the 90 mass % alcohol solutions demonstrate thermal decomposition traces

https://doi.org/10.1021/acssuschemeng.5c01554
ACS Sustainable Chem. Eng. 2025, 13, 7549−7561

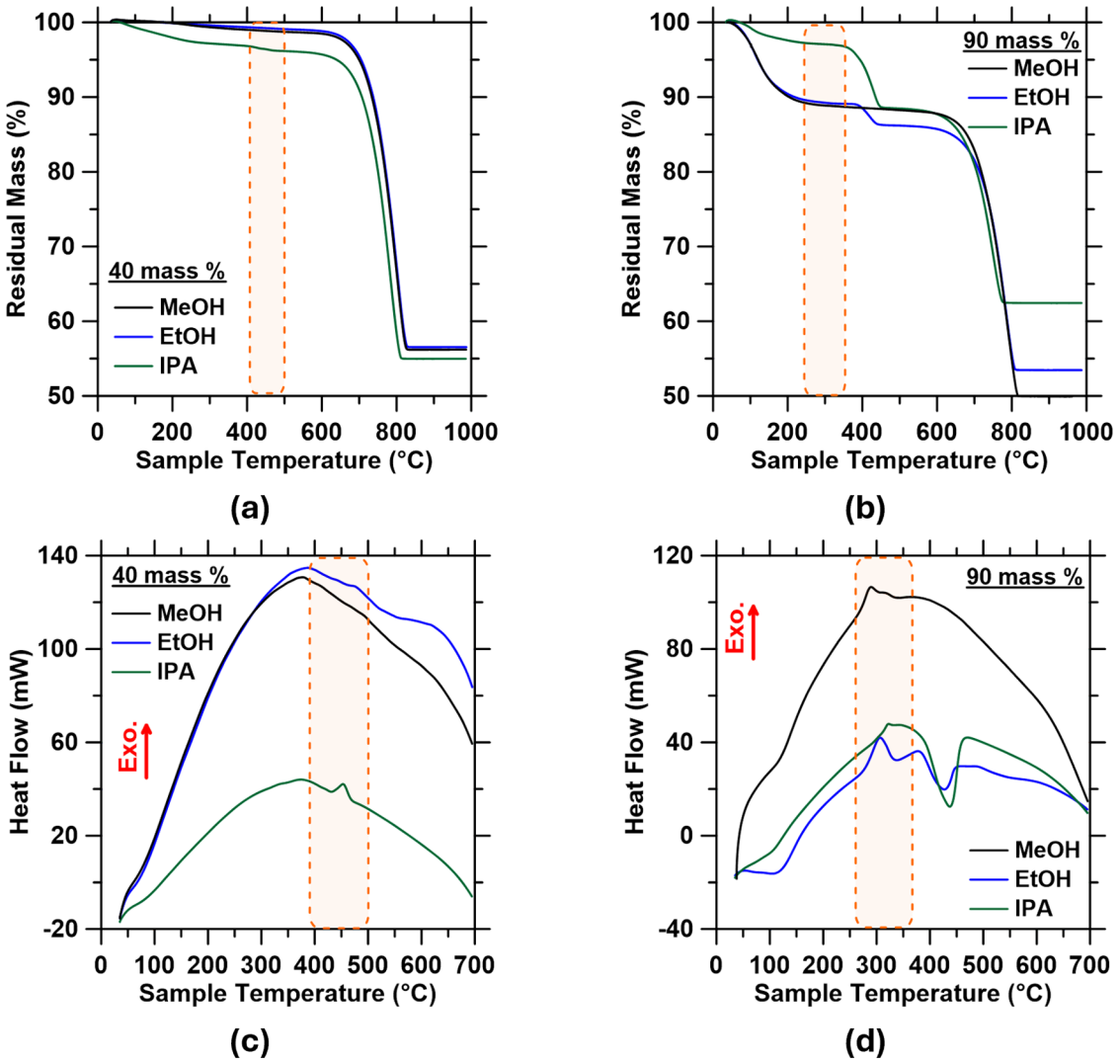

Figure 4. Representative mass loss curves of the precipitates synthesized in (a) 40 mass %, and (b) 90 mass % alcohol solutions. The corresponding heat flow curves (c, d) were truncated to highlight the exothermic peaks in each sample.

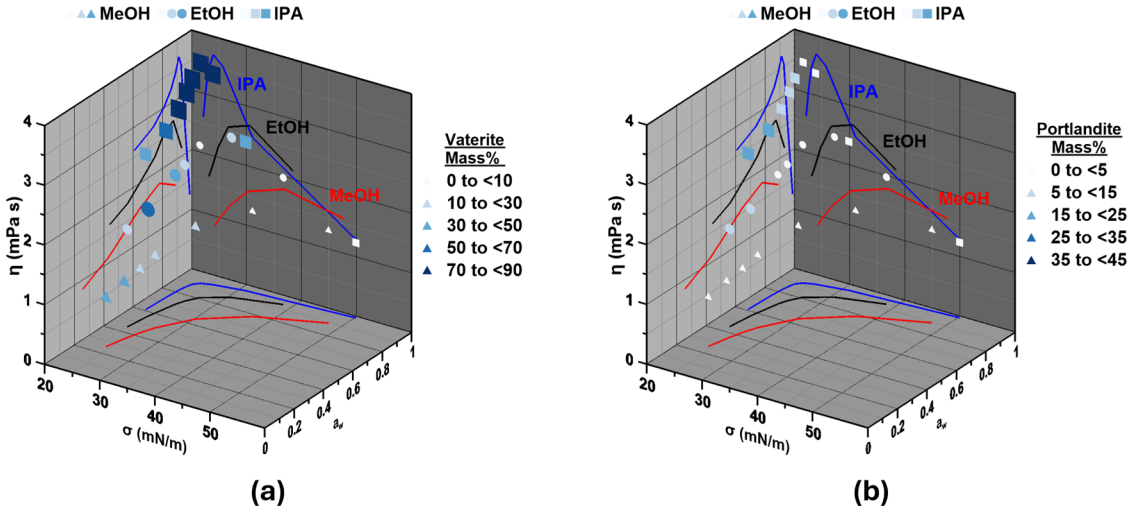

Figure 5. Mass composition of (a) vaterite and (b) unreacted portlandite in the precipitate as a function of η, σ, and a_w for each alcohol type. The symbol colors and size vary with the composition of a given component (i.e., a higher composition is indicated by a larger symbol size and a darker color). The lines projected on each plane show the dependence of one parameter as a function of the other (e.g., change in η as a function of a_w). A summary of this data is provided in Tables S7 and S8.

https://doi.org/10.1021/acssuschemeng.5c01554
ACS Sustainable Chem. Eng. 2025, 13, 7549−7561

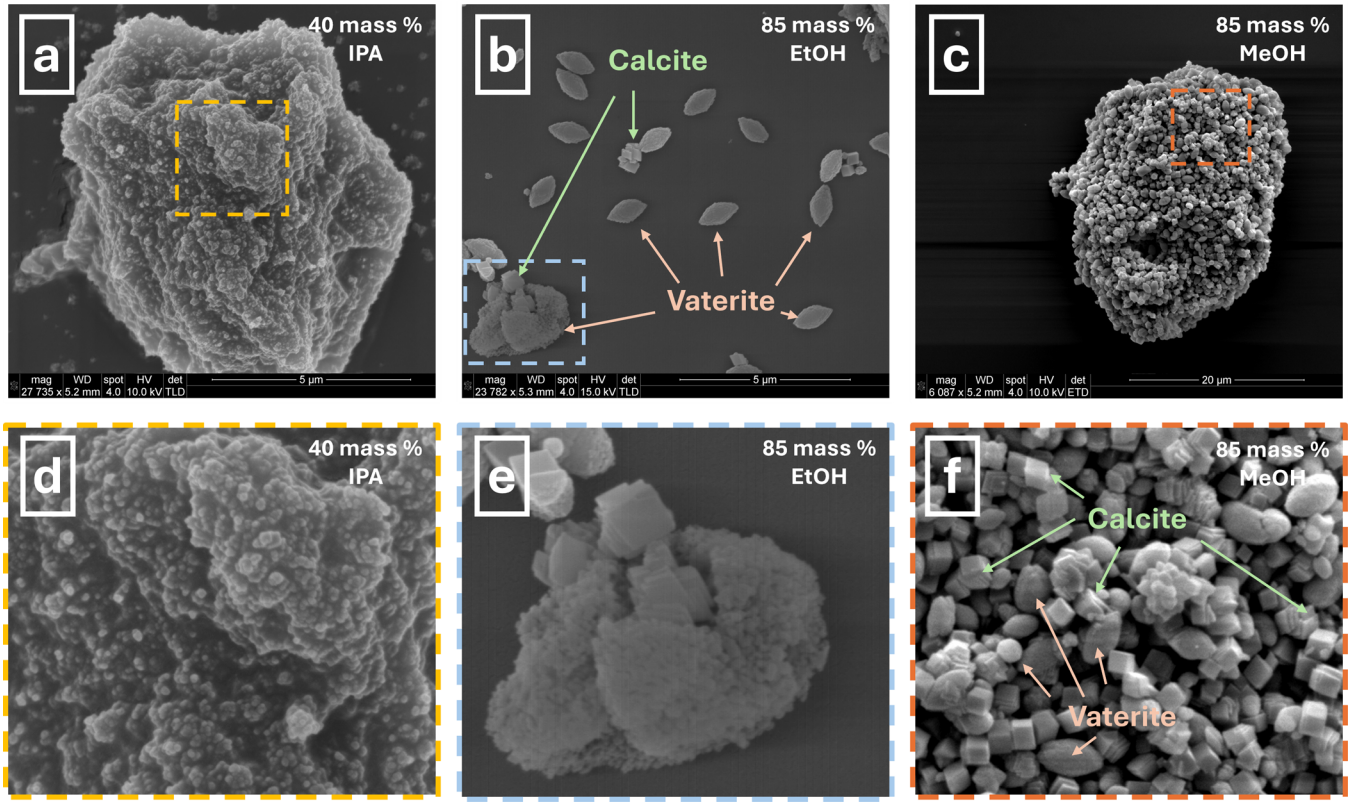

Figure 6. Representative SEM images of the precipitates formed in (a, d) IPA, (b, e) EtOH, and (c, f) MeOH as additives. Vaterite and calcite clusters are denoted except in images (a, c) due to the high vaterite content of the sample, as shown in the corresponding IR spectra of the precipitates (see Figure S9).

that are characteristic of ACC. Generally, ACC is categorized as a hydrous form of $CaCO_3$, hence, its decomposition proceeds with an initial mass loss below 200 °C (e.g., see Figure 4b) followed by a sequential exothermic peak at ~300 °C, indicating ACC crystallization (as shown in Figure 4d).[57,58] On the other hand, the exothermic peak associated with the thermally induced transformation of vaterite into calcite generally occurs above 400 °C without a preceding mass loss below 200 °C, as shown in Figure 4(a),4(c), respectively.[59,60] Although the effect of water activity is as expected, the differences observed across the alcohol types suggest that a_w alone is not a suitable marker that is indicative of vaterite formation. Interestingly, Figure 3(a) shows that a greater decrease in the calcite content (and portlandite conversion) for a smaller change in a_w (i.e., lower additive concentration) was observed for the larger alcohols. Thus, a greater inhibition of further dissolution of reactant and calcite formation was observed for IPA as compared to methanol and ethanol.

Influence of Viscosity (η) and Surface Tension (σ). An interesting observation that emerges when η and σ are considered simultaneously is that vaterite's selectivity substantially increases when σ < 30 mN/m and η > 2 mPa·s as shown in Figure 5(a). To consider the concurrent effects of the three variables (i.e., a_w, η, or σ) on vaterite formation, the collection of experimental data was analyzed using a response surface method (RSM). A sequential sum of the squares method that considers two-factor interactions (e.g., water activity and viscosity, and surface tension and viscosity) with a backward regression procedure was used. This regression removes parameters in the design model (see eq 7) with significant p-values, which indicates a greater probability of occurrence under the null hypothesis that the parameter has no influence at all. Here, parameters with p-values <0.05 indicate a very low probability that the null hypothesis is correct. The interaction between σ and η (p-value = 0.0094) was identified as a significant parameter, while σ (p-value = 0.079) and the interaction between a_w and η (p-value = 0.062) were somewhat significant. In contrast, no apparent link between a_w (p-value = 0.45) and the tendency for vaterite formation was determined. The lack of a clear relationship is on account of a greater change in η and σ with increasing molecular weight of the alcohol, as shown in Table S3. As a result, for a solution with 20 mass % alcohol, the surface tension at 20 °C is about 48, 39, and 31 mN/m with MeOH (a_w = 0.89), EtOH (a_w = 0.93), and IPA (a_w = 0.95), respectively.[61] A similar trend is observed with η (see Table S3), for which the η of the 20 mass % IPA is 1.6x of the 20 mass % MeOH. Thus, a lower concentration of IPA induces a greater effect on the solution's properties than the other alcohols. This complex and nonlinear relationship arises on account of the varying clustering behaviors of alcohol and water, which vary as a function of the alcohol type, the temperature, and the mass fractions of the alcohol−water mixture.[62,63]

$$\text{vaterite (mass \%)} = 33.37 - 104.02a_w + 2.38\sigma + 15.55\eta + 80.46a_w\eta - 2.68\sigma\eta \quad (7)$$

It should be noted that η and σ can also alter bubble morphology (i.e., size, shape, and swarm size) and gas holdup times. More specifically, an increase in alcohol concentration leads to a reduction in σ and a slight increase in η, which

https://doi.org/10.1021/acssuschemeng.5c01554
ACS Sustainable Chem. Eng. 2025, 13, 7549−7561

results in the formation of smaller bubbles (i.e., greater surface area to volume ratio) with lower rising velocities.[55,64,65] This reduction in bubble size may explain the nanocrystalline habit of the vaterite formed in IPA (see Figures 6(d) and S11). Previous studies postulate that the morphology of the synthesized $CaCO_3$ is dictated by the morphology of the bubble, mass transfer of CO_2, and efficiency of mixing in the reactor, which may imply that nucleation initiates on the bubble surface.[66,67] In contrast to the nanoscale precipitates from the IPA system, larger spindle-shaped vaterite particulates were formed with 85 mass % EtOH and MeOH additives as shown in Figure 6(b,c), respectively. The formation of this particular morphology is correlated with a Ca^{2+} deficient system with a $[CO_3^{2-}]/[Ca^{2+}]$ ratio of ∼2 to 3 whereas the nanocrystalline habit of the precipitated vaterite with IPA (shown in Figure 6(a),6(d)) was associated with an even more extreme condition of $[CO_3^{2-}]/[Ca^{2+}] > 10$ and rapid mixing.[68,69] These latter conditions may be achieved as water is replaced with alcohol, such that Ca^{2+} species preferentially interact with alcohol, which raises the relative amount of carbonate available in solution, per unit of mobile-Ca that is available.

Assessing the "Solution Properties" Hypothesis. The experimental results suggest that η and σ may be leveraged to control vaterite selectivity. To assess the validity of this hypothesis, two other alcohols, n-propanol (n-Pr) and tert-butyl alcohol (tBA), were tested at concentrations summarized in Table S9. These alcohols were selected due to their structural similarity (i.e., single hydroxyl and short carbon chain) with the three alcohols that were assessed and full miscibility in water. As such, the alcohol concentration can be leveraged to tailor the solution properties to fit the region of interest. For this comparison, mixtures with $\sigma < 30$ mN/m and $\eta > 2$ mPa·s were produced. Despite the similarity in macroscopic properties of the (solution) mixtures, Figure 7 shows a distinct superiority of IPA in enhancing vaterite selectivity that renders control of the solution properties as an insufficient mechanism to explain the selectivity. A possible explanation for this may be rooted in the difference in solvation behaviors of the ion species (i.e., Ca^{2+} and CO_3^{2-}) in the solvent mixture (i.e., alcohol and water). More specifically, the lower electric charge density of CO_3^{2-} (17 C/mm^3) is better solvated in water, whereas electrically charge dense Ca^{2+} (52 C/mm^3) can be solvated in both alcohol and water.[30,46,70] Previous authors hypothesize that the alcohol in the solvated layer around Ca^{2+} reduces the desolvation energy for $CaCO_3$ crystallization (i.e., lowering the activation energy of crystallization), thus favoring the formation of metastable phases like vaterite.[46,71] However, as Xiao et al. demonstrated, Ca^{2+} − alcohol coordination is also important to producing a CO_3^{2-} rich solution and maximizing vaterite formation.[30] Hence, the exclusive precipitation of calcite with weakly polar tBA (E_T^N = 0.389 kcal/mol) is likely a function of its lower coordination with Ca^{2+}.[72] On the other hand, the greater vaterite selectivity with IPA (E_T^N = 0.546 kcal/mol) despite its lower polarity than MeOH (E_T^N = 0.762 kcal/mol), EtOH (E_T^N = 0.654 kcal/mol), and nPr (E_T^N = 0.617 kcal/mol) suggests a balance between Ca^{2+}−alcohol coordination and the ion-desolvation (dehydration) energy.[72]

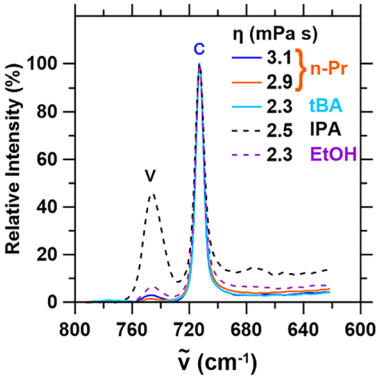

Figure 7. Representative IR spectra of the precipitates as a function of the solution viscosity (η) of a given alcohol solution. A summary of the alcohol compositions and the macroscopic properties of the mixture is provided in Table S9. The unique peaks corresponding to vaterite ("V") and calcite ("C") are denoted.

The observed nonlinearity in vaterite selectivity as a function of both alcohol type and composition (see Figure S12) indicates a complex behavior, which could be related to the influence of the ion−solvent interactions on the formation of the amorphous $CaCO_3$ precursor, i.e., the prenucleation cluster that holds the imprint of the final precipitate, and its subsequent crystallization.[4,73] Given that a reduction in crystallinity (i.e., higher ACC content) was observed alongside greater vaterite formation (see the diffraction pattern and IR spectra in Figures S7 and S8, respectively), the crystallization process appears to proceed from the initial formation of an ACC with a proto-vaterite structure as previous authors have observed in pure isopropanol systems.[24,74] The alcohol in the solvation layer of Ca^{2+} cations is thought to affect the structure of these proto-crystalline clusters by restricting the mobility and incorporation of water into the structure. However, this structure likely does not have a single form (i.e., it may be nonunique) as the solvation structure around Ca^{2+} is known to vary not only as a function of the alcohol type but also the concentration of alcohol and ion species (e.g., Ca^{2+}, CO_3^{2-}, and Cl^-) in solution.[46,50,75] While there are several important clues that emerge, it should also be recognized that direct elaboration of the reaction mechanism of vaterite's stabilization in IPA-water mixtures remains challenging. For example, at high alcohol concentrations (>80 mol % alcohol), a reaction pathway that includes the partial formation of intermediary Ca − alkoxide species that may favorably form vaterite emerges.[76,77] Other authors have also proposed the simultaneous occurrence of solid − solid transformation and dissolution and recrystallization during ACC crystallization in the presence of IPA.[74] In addition, Zhang et al. hypothesized that the aggregation behavior (i.e., particle morphology) and stability of the precipitates were determined by the excess ion species in solution.[46] For instance, in a CO_3^{2-}-excess system, the precipitates will "inherit" the water-rich layer of CO_3^{2-}. If the bulk alcohol concentration is high, the large interfacial energy difference between the water-rich particle surface and the alcohol-rich bulk will induce directional crystal growth according to the alcohol structure of the solution.[46] In general, the influence of different alcohols on $CaCO_3$'s polymorphism and morphology was found to be largely dependent on the stirring (convection, mixing) conditions and alcohol's concentration, rather than the alcohol type.[27,78] This may indicate that the specific affinity of the alcohol to a given $CaCO_3$ polymorph is a relevant factor to consider, as it determines the formation and resulting stability of the precipitate in solution. In particular, for IPA, some authors have hypothesized that

https://doi.org/10.1021/acssuschemeng.5c01554
ACS Sustainable Chem. Eng. 2025, 13, 7549−7561

vaterite precipitation is driven by the greater propensity of IPA to stabilize the (001) facet of vaterite, while others attribute this to its stronger interaction with calcite.[23,24] However, the exact mechanism that results in the selectivity toward a particular polymorph in a given alcohol solution remains unclear.[27,78] While direct and unambiguous evidence related to the mechanisms of how IPA affects polymorph selection and stability of $CaCO_3$ remains unclear, it is reasonable to conclude that the mechanism(s) are complex and multiphase, i.e., imposed on and via the solution and the precipitate(s). Better elaboration of this mechanism(s) remains an important goal − to build a better understanding of pathways that enable chemical control of polymorph selection and stability across mineral compositions and systems.

SUMMARY AND CONCLUSIONS

This paper has shown that IPA mediates the rapid and selective synthesis of vaterite in aqueous solution using $Ca(OH)_2$ and a dilute CO_2 stream (5 vol %) as reactants. While several additives, e.g., including methanol, ethanol, and sucrose, enable vaterite formation, IPA enables the production of vaterite at exceptional selectivity (>80 mass %) that is unmatched by any other additive in this study. While it appeared as though a "Goldilocks region" of solution (i.e., alcohol + water) properties, i.e., surface tension (σ < 30 mN/m) and the viscosity (η > 2 mPa·s), would favor the formation of vaterite in the presence of monohydric alcohols—this suggestion was unfounded. For example, the lower vaterite selectivity in n-propanol and tert-butyl alcohol solutions in the supposed "Goldilocks region", as compared to IPA mixtures, is indicative of a more complex interaction between the ion species and solvent mixture (i.e., alcohol and water). More specifically, it is indicated that the solvation behavior of ion species in the presence of the different alcohols influences ion and water interactions, including desolvation, and transport during $CaCO_3$ crystallization. The observed formation of ACC alongside vaterite suggests that the ion − alcohol interaction influences the proto-crystalline structures of the ACC, and the subsequent stability of the metastable species formed (i.e., ACC, vaterite).

Implications Toward a Continuous Method for Producing Vaterite. The proposed IPA-mediated vaterite synthesis approach presents opportunities to use zero-carbon lime (e.g., produced by the ZeroCal process), and CO_2 bearing flue gases to produce vaterite at scale.[16] The mediator role of IPA fulfilled in this system is important in that, since IPA is not consumed during the reaction, it can be readily recovered and reused, e.g., by extractive distillation or a hybrid vapor permeation−distillation method.[79] Importantly, given that the optimal IPA concentration to maximize vaterite's yield and selectivity is in the range of 30−60 mass % (IPA), it suggests that direct recycling of the mixed solution could be realized—thereby enabling the design of a simple continuous process. It is also important to highlight that given the dual role of IPA in the selective precipitation and continued stabilization of vaterite, synthesized particulates that were stored at ambient conditions (T: ∼ 20 °C, RH: 50−60%) remain stable even after extensive periods of storage, up to 3 years (as shown in Figure S13). That said, to assess the feasibility of the approach at scale, and verify the sustainability of the process. it is important to consider in more lifecycle detail: the embodied carbon intensity of IPA production (1.85 t_{CO2}/t_{IPA}), the extent of cyclic reuse and recovery of IPA during vaterite production, the energy intensity of the production process, the grid − mx of electricity that is utilized, and consequently the extent of net amount of CO_2 utilization/reduction that is realized.[80] In addition, further questions remain about how and why IPA offers an unmatched ability to affect the selectivity and yield of vaterite formation, which is superior to other additives, and a better understanding of these aspects would further improve our synthesis routes.

ASSOCIATED CONTENT

Supporting Information

The Supporting Information is available free of charge at https://pubs.acs.org/doi/10.1021/acssuschemeng.5c01554.

Analysis of the hydrated lime reactant (Figure S1); precipitated particulates (Table S1) and gas phase concentration of CO_2 (Figure S2); summary of the additives used and the estimated a_w, ΔH_{Mix}, σ, and η of the mixed solutions (Tables S2−S3; S9); detailed explanation of the thermodynamic modeling approach and the results (Figures S3−S4; Table S5); methodology used to calculate the a_w for the various alcohol mixtures (Table S4; Equations S1−S3) and to determine the rate constants (Figures S5−S6; Table S6; Equations S5−S9); XRD patterns (Figure S7); IR spectra (Figures S8−S9) and SEM images (Figures S10−S11) of the particulates precipitated in solutions with variable alcohol type and concentration; A detailed summary of QXRD and TGA results as a function of the macroscopic properties of the alcohol solutions (Table S7) and alcohol type and concentration (Table S8; Figure S12); Influence of ambient storage on vaterite stability (Figure S13) (PDF)

AUTHOR INFORMATION

Corresponding Author

Gaurav Sant − *Institute for Carbon Management, University of California, Los Angeles, Los Angeles 90095 California, United States; Department of Civil and Environmental Engineering, California Nanosystems Institute (CNSI), and Department of Materials Science and Engineering, University of California, Los Angeles, Los Angeles 90095 California, United States;* orcid.org/0000-0002-1124-5498; Email: gsant@ucla.edu

Authors

Jenny Arabit − *Institute for Carbon Management, University of California, Los Angeles, Los Angeles 90095 California, United States; Department of Chemical and Biomolecular Engineering, University of California, Los Angeles, Los Angeles 90095 California, United States;* orcid.org/0000-0003-1341-6518

Dale Prentice − *Institute for Carbon Management, University of California, Los Angeles, Los Angeles 90095 California, United States; Department of Civil and Environmental Engineering, University of California, Los Angeles, Los Angeles 90095 California, United States*

Justin Luong − *Department of Chemical and Biomolecular Engineering, University of California, Los Angeles, Los Angeles 90095 California, United States*

Arnaud Bouissonnié − *Institute for Carbon Management, University of California, Los Angeles, Los Angeles 90095*

https://doi.org/10.1021/acssuschemeng.5c01554
ACS Sustainable Chem. Eng. 2025, 13, 7549−7561

California, United States; orcid.org/0000-0003-4590-5631

Jagannathan Govindhakannan − *Institute for Carbon Management, University of California, Los Angeles, Los Angeles 90095 California, United States*

Fabian Rosner − *Institute for Carbon Management, University of California, Los Angeles, Los Angeles 90095 California, United States; Department of Civil and Environmental Engineering, University of California, Los Angeles, Los Angeles 90095 California, United States*

Dante Simonetti − *Institute for Carbon Management, University of California, Los Angeles, Los Angeles 90095 California, United States; Department of Chemical and Biomolecular Engineering, University of California, Los Angeles, Los Angeles 90095 California, United States;* orcid.org/0000-0002-5708-460X

Erika La Plante − *Department of Material Science and Engineering, University of California, Davis, Davis 95616 California, United States;* orcid.org/0000-0002-5273-9523

Torben Gadt − *Department of Chemistry, Technical University of Munich, Lehrstuhl für Bauchemie, D-85747 Garching bei München, Germany;* orcid.org/0000-0001-7940-5403

Complete contact information is available at: https://pubs.acs.org/10.1021/acssuschemeng.5c01554

Notes

The authors declare no competing financial interest.

■ ACKNOWLEDGMENTS

The authors acknowledge financial support provided by The Chan-Zuckerberg Initiative (CZI)/Chan-Zuckerberg Initiative Foundation (CZIF), The Grantham Foundation for the Protection of the Environment, and UCLA's Institute for Carbon Management. The authors would also like to acknowledge Dr. Marie Collin (UCLA and TU-Munich) for providing critical feedback regarding the experimental approach and methodology used herein. The contents of this paper reflect the views and opinions of the authors, who are responsible for the accuracy of the datasets presented herein.

■ REFERENCES

(1) U.S. Department of Energy (DOE). Pathways to Commercial Liftoff: Low-Carbon Cement 2023 https://liftoff.energy.gov/wp-content/uploads/2023/12/20230921-Pathways-to-Commercial-Liftoff-Cement.pdf (accessed April 07, 2025).

(2) Hatfield, A. *Cement. Mineral Commodity Summaries 2024: U.S. Geological Surveys*; 2024; pp 54−55.

(3) Kellermeier, M.; Raiteri, P.; Berg, J. K.; Kempter, A.; Gale, J. D.; Gebauer, D. Entropy Drives Calcium Carbonate Ion Association. *ChemPhysChem* **2016**, *17* (21), 3535−3541.

(4) Balodis, M.; Rao, Y.; Stevanato, G.; Kellner, M.; Meibom, J.; Negroni, M.; Chmelka, B. F.; Emsley, L. Observation of Transient Prenucleation Species of Calcium Carbonate by DNP-Enhanced NMR. *J. Phys. Chem. Lett.* **2024**, *15* (31), 7954−7961.

(5) Avaro, J.; Moon, E. M.; Schulz, K. G.; Rose, A. L. Calcium Carbonate Prenucleation Cluster Pathway Observed via In Situ Small-Angle X-Ray Scattering. *J. Phys. Chem. Lett.* **2023**, *14*, 4517−4523.

(6) Du, H.; Amstad, E. Water: How Does It Influence the CaCO3 Formation? *Angew. Chem., Int. Ed.* **2020**, *59* (5), 1798−1816.

(7) Falzone, G.; Mehdipour, I.; Neithalath, N.; Bauchy, M.; Simonetti, D.; Sant, G. New Insights into the Mechanisms of Carbon Dioxide Mineralization by Portlandite. *AIChE J.* **2021**, *67* (5), No. e17160.

(8) Liendo, F.; Arduino, M.; Deorsola, F. A.; Bensaid, S. Factors Controlling and Influencing Polymorphism, Morphology and Size of Calcium Carbonate Synthesized through the Carbonation Route: A Review. *Powder Technol.* **2022**, *398*, No. 117050.

(9) Hargis, C. W.; Chen, I.; Wang, Y.; Maraghechi, H.; Gilliam, R. J.; Monteiro, P. J. M. Microstructure Development of Calcium Carbonate Cement through Polymorphic Transformations. *Cement Concr. Compos.* **2024**, *153*, No. 105715.

(10) Hargis, C. W.; Chen, I. A.; Devenney, M.; Fernandez, M. J.; Gilliam, R. J.; Thatcher, R. P. Calcium Carbonate Cement: A Carbon Capture, Utilization, and Storage (CCUS) Technique. *Materials* **2021**, *14* (11), 2709.

(11) Li, Y.; Li, Y.; Ma, H.; Li, J. The Hydration, Microstructure, and Mechanical Properties of Vaterite Calcined Clay Cement (VC 3). *Cement Concr. Res.* **2024**, *175*, No. 107374.

(12) Nehrke, G.; Van Cappellen, P. Framboidal Vaterite Aggregates and Their Transformation into Calcite: A Morphological Study. *J. Cryst. Growth* **2006**, *287*, 528−530.

(13) Plummer, L. N.; Busenberg, E. The Solubilities of Calcite, Aragonite and Vaterite in CO2-H2O Solutions between 0 and 90°C, and an Evaluation of the Aqueous Model for the System CaCO3-CO2-H2O. *Geochim. Cosmochim. Acta* **1982**, *46* (6), 1011−1040.

(14) Trushina, D. B.; Bukreeva, T. V.; Kovalchuk, M. V.; Antipina, M. N. CaCO3 Vaterite Microparticles for Biomedical and Personal Care Applications. *Mater. Sci. Eng.: C* **2014**, *45*, 644−658.

(15) Brečević, L.; Kralj, D. On Calcium Carbonates: From Fundamental Research to Application. *Croat. Chem. Acta* **2007**, *80* (3−4), 467−484.

(16) Leão, A.; Collin, M.; Ghodkhande, S.; Bouissonnié, A.; Chen, X.; Malin, B.; Liu, Y.; Hovey, G.; Govindhakannan, J.; Plante, E. La.; Jassby, D.; Gädt, T.; Corsini, L.; Simonetti, D.; Rosner, F.; Sant, G. ZeroCAL: Eliminating Carbon Dioxide Emissions from Limestone's Decomposition to Decarbonize Cement Production *ACS Sustainable Chem. Eng.*, 15762 15787 DOI: 10.1021/acssuschemeng.4c03193.

(17) Songolzadeh, M.; Soleimani, M.; Takht Ravanchi, M.; Songolzadeh, R. Carbon Dioxide Separation from Flue Gases: A Technological Review Emphasizing Reduction in Greenhouse Gas Emissions. *Scientific World J.* **2014**, *2014*, 828131.

(18) Chuajiw, W.; Takatori, K.; Igarashi, T.; Hara, H.; Fukushima, Y. The Influence of Aliphatic Amines, Diamines, and Amino Acids on the Polymorph of Calcium Carbonate Precipitated by the Introduction of Carbon Dioxide Gas into Calcium Hydroxide Aqueous Suspensions. *J. Crystal Growth* **2013**, *386*, 119−127, DOI: 10.1016/j.jcrysgro.2013.10.009.

(19) Pouget, E. M.; Bomans, P. H. H.; Dey, A.; Frederik, P. M.; De With, G.; Sommerdijk, N. A. J. M. The Development of Morphology and Structure in Hexagonal Vaterite. *J. Am. Chem. Soc.* **2010**, *132* (33), 11560−11565.

(20) Said, A.; Laukkanen, T.; Järvinen, M. Pilot-Scale Experimental Work on Carbon Dioxide Sequestration Using Steelmaking Slag. *Appl. Energy* **2016**, *177*, 602−611.

(21) Hamouda, A. S.; Eldien, M. S.; Abadir, M. F. Carbon Dioxide Capture by Ammonium Hydroxide Solution and Its Possible Application in Cement Industry. *Ain Shams Eng. J.* **2020**, *11* (4), 1061−1067.

(22) Clark, K. G.; Hetherington, H. C. The Heat of Formation of Ammonium Carbamate from Ammonia and Carbon Dioxide. *J. Am. Chem. Soc.* **1927**, *49* (8), 1909−1915.

(23) Konopacka-Łyskawa, D.; Czaplicka, N.; Łapiński, M.; Kościelska, B.; Bray, R. Precipitation and Transformation of Vaterite Calcium Carbonate in the Presence of Some Organic Solvents. *Materials* **2020**, *13* (12), 1−14.

(24) Zhang, Y.; Qiao, L.; Yan, H.; Zizak, I.; Zaslansky, P.; Li, Y.; Qi, L.; Ma, Y. Vaterite Microdisc Mesocrystals Exposing the (001) Facet Formed via Transformation from Proto-Vaterite Amorphous Calcium Carbonate. *Cryst. Growth Des.* **2020**, *20* (5), 3482−3492.

(25) Ishikawa, K.; Freitas, P.; Kishida, R.; Hayashi, K.; Tsuchiya, A. Fabrication of Vaterite Blocks from a Calcium Hydroxide Compact. *Ceram. Int.* **2022**, *48* (3), 4153−4157.
(26) Kim, G.; Kim, S.; Kim, M. J. Effect of Sucrose on CO2 Storage, Vaterite Content, and CaCO3 Particle Size in Indirect Carbonation Using Seawater. *J. CO2 Util.* **2022**, *57*, No. 101894.
(27) Sand, K. K.; Rodriguez-Blanco, J. D.; Makovicky, E.; Benning, L. G.; Stipp, S. L. S. Crystallization of CaCO 3 in Water-Alcohol Mixtures: Spherulitic Growth, Polymorph Stabilization, and Morphology Change. *Cryst. Growth Des.* **2012**, *12* (2), 842−853.
(28) Pérez-Villarejo, L.; Takabait, F.; Mahtout, L.; Carrasco-Hurtado, B.; Eliche-Quesada, D.; Sánchez-Soto, P. J. Synthesis of Vaterite CaCO3 as Submicron and Nanosized Particles Using Inorganic Precursors and Sucrose in Aqueous Medium. *Ceram. Int.* **2018**, *44* (5), 5291−5296.
(29) Siva, T.; Muralidharan, S.; Sathiyanarayanan, S.; Manikandan, E.; Jayachandran, M. Enhanced Polymer Induced Precipitation of Polymorphous in Calcium Carbonate: Calcite Aragonite Vaterite Phases. *J. Inorg. Organomet Polym. Mater.* **2017**, *27*, 770−778.
(30) Xiao, H.; Hu, C.; Chen, C.; Tao, C.; Wu, Y.; Jiang, J. The Advantage of Alcohol−Calcium Method on the Formation and the Stability of Vaterite against Ethanol−Water Binary Solvent Method. *J. Mater. Res.* **2020**, *35* (3), 289−298.
(31) Rodriguez-Blanco, J. D.; Sand, K. K.; Benning, L. G.ACC and Vaterite as Intermediates in the Solution-Based Crystallization of CaCO. In *New Perspectives on Mineral Nucleation and Growth*, 2017; pp 93−111.
(32) Seo, K. S.; Han, C.; Wee, J. H.; Park, J. K.; Ahn, J. W. Synthesis of Calcium Carbonate in a Pure Ethanol and Aqueous Ethanol Solution as the Solvent. *J. Cryst. Growth* **2005**, *276* (3−4), 680−687.
(33) Trushina, D. B.; Bukreeva, T. V.; Antipina, M. N. Size-Controlled Synthesis of Vaterite Calcium Carbonate by the Mixing Method: Aiming for Nanosized Particles. *Cryst. Growth Des.* **2016**, *16* (3), 1311−1319.
(34) Xu, B.; Poduska, K. M. Linking Crystal Structure with Temperature-Sensitive Vibrational Modes in Calcium Carbonate Minerals. *Phys. Chem. Chem. Phys.* **2014**, *16* (33), 17634−17639.
(35) Liu, R.; Huang, S.; Zhang, X.; Song, Y.; He, G.; Wang, Z.; Lian, B. Bio-Mineralisation, Characterization, and Stability of Calcium Carbonate Containing Organic Matter †. *RSC Adv.* **2021**, *11*, 14415−14425, DOI: 10.1039/d1ra00615k.
(36) Farhadi Khouzani, M.; Chevrier, D. M.; Güttlein, P.; Hauser, K.; Zhang, P.; Hedin, N.; Gebauer, D. Disordered Amorphous Calcium Carbonate from Direct Precipitation. *CrystEngComm* **2015**, *17* (26), 4842−4849.
(37) Al Omari, M. M. H.; Rashid, I. S.; Qinna, N. A.; Jaber, A. M.; Badwan, A. A. Chapter Two: Calcium Carbonate. In *Profiles of Drug Substances, Excipients and Related Methodology*; Academic Press, 2016; Vol. *41*, pp 31−132.
(38) Doebelin, N.; Kleeberg, R. Profex: A Graphical User Interface for the Rietveld Refinement Program BGMN. *J. Appl. Crystallogr.* **2015**, *48*, 1573−1580.
(39) Gražulis, S.; Daškevič, A.; Merkys, A.; Chateigner, D.; Lutterotti, L.; Quirós, M.; Serebryanaya, N. R.; Moeck, P.; Downs, R. T.; Le Bail, A. Crystallography Open Database (COD): An Open-Access Collection of Crystal Structures and Platform for World-Wide Collaboration. *Nucleic Acids Res.* **2012**, *40* (D1), D420−D427.
(40) Lothenbach, B.; Durdziński, P.; De Weerdt, K. Thermogravimetric Analysis. In *A Practical Guide to Microstructural Analysis of Cementitious Materials*; CRC Press: Boca Raton, 2018; pp 178−211.
(41) Munawaroh, F.; Khamsatul Muharrami, L.; Arifin, Z. The Effect of CO2 Gas Flow Rate on Precipitated CaCO3 Formed at Room Temperature. In *AIP Conference Proceedings*, 2014; p 30018.
(42) García Carmona, J.; Gómez Morales, J.; Rodríguez Clemente, R. Rhombohedral−Scalenohedral Calcite Transition Produced by Adjusting the Solution Electrical Conductivity in the System Ca(OH)2−CO2−H2O. *J. Colloid Interface Sci.* **2003**, *261* (2), 434−440.
(43) Wachi, S.; Jones, A. G. Effect of Gas-Liquid Mass Transfer on Crystal Size Distribution during the Batch Precipitation of Calcium Carbonate. *Chem. Eng. Sci.* **1991**, *46* (12), 3289−3293.
(44) Erdemir, D.; Squibb, B.-M.; Lee, A. Y. Crystal Nucleation. In *Handbook of Industrial Crystallization*; Cambridge University Press: Cambridge, 2019; pp 76−114.
(45) Niu, Y. Q.; Liu, J. H.; Aymonier, C.; Fermani, S.; Kralj, D.; Falini, G.; Zhou, C. H. Calcium Carbonate: Controlled Synthesis, Surface Functionalization, and Nanostructured Materials. *Chem. Soc. Rev.* **2022**, *51* (18), 7883−7943.
(46) Zhang, L.; Yue, L. H.; Wang, F.; Wang, Q. Divisive Effect of Alcohol−Water Mixed Solvents on Growth Morphology of Calcium Carbonate Crystals. *J. Phys. Chem. B* **2008**, *112* (34), 10668−10674.
(47) Vázquez, G.; Chenlo, F.; Pereira, G. Enhancement of the Absorption of CO2 in Alkaline Buffers by Organic Solutes: Relation with Degree of Dissociation and Molecular OH Density. *Ind. Eng. Chem. Res.* **1997**, *36* (6), 2353−2358.
(48) Sánchez-Cantú, M.; Reyes-Cruz, F. M.; Rubio-Rosas, E.; Pérez-Díaz, L. M.; Ramírez, E.; Valente, J. S. Direct Synthesis of Calcium Diglyceroxide from Hydrated Lime and Glycerol and Its Evaluation in the Transesterification Reaction. *Fuel* **2014**, *138*, 126−133.
(49) Yu, M.; Kang, X.; Qian, L. Interactions between Monovalent Cations and Polyethylene Glycol: A Study at Micro Level. *Colloids Surf. A Physicochem Eng. Asp* **2024**, *680*, No. 132731.
(50) Ren, G.; Ha, Y.; Liu, Y. S.; Feng, X.; Zhang, N.; Yu, P.; Zhang, L.; Yang, W.; Feng, J.; Guo, J.; Liu, X. Deciphering the Solvent Effect for the Solvation Structure of Ca2+ in Polar Molecular Liquids. *J. Phys. Chem. B* **2020**, *124* (16), 3408−3417.
(51) Mei, L.-H.; Lin, D.-Q.; Zhu, Z.-Q.; Han, Z.-X. Densities and Viscosities of Polyethylene Glycol + Salt + Water Systems at 20 °C. *J. Chem. Eng. Data* **1995**, *40*, 1168−1171.
(52) Amooey, A. A.; Fazlollahnejad, M. Study of Surface Tension of Binary Mixtures of Poly (Ethylene Glycol) in Water and Poly (Propylene Glycol) in Ethanol and Its Modeling Using Neural Network. *Iranian J. Chem. Eng. (IJChE)* **2014**, *11* (1), 19−29.
(53) Vazquez, G.; Alvarez, E.; Navaza, J. M. Surface Tension of Alcohol + Water from 20 to 50 °C. *J. Chem. Eng. Data* **1995**, *40* (3), 611−614.
(54) Wang, Z.; Guo, K.; Liu, H.; Liu, C.; Geng, Y.; Lu, Z.; Jiao, B.; Chen, D. Effects of Bubble Size on the Gas−Liquid Mass Transfer of Bubble Swarms with Sauter Mean Diameters of 0.38−4.88 Mm in a Co-Current Upflow Bubble Column. *J. Chem. Technol. Biotechnol.* **2020**, *95* (11), 2853−2867.
(55) Basařová, P.; Pišlová, J.; Mills, J.; Orvalho, S. Influence of Molecular Structure of Alcohol-Water Mixtures on Bubble Behaviour and Bubble Surface Mobility. *Chem. Eng. Sci.* **2018**, *192*, 74−84.
(56) Hu, B.; Nienow, A. W.; Hugh Stitt, E.; Pacek, A. W. Bubble Sizes in Agitated Solvent/Reactant Mixtures Used in Heterogeneous Catalytic Hydrogenation of 2-Butyne-1,4-Diol. *Chem. Eng. Sci.* **2006**, *61* (20), 6765−6774.
(57) Albéric, M.; Bertinetti, L.; Zou, Z.; Fratzl, P.; Habraken, W.; Politi, Y. The Crystallization of Amorphous Calcium Carbonate Is Kinetically Governed by Ion Impurities and Water. *Adv. Sci.* **2018**, *5* (5), 1701000 DOI: 10.1002/advs.201701000.
(58) Günther, C.; Becker, A.; Wolf, G.; Epple, M. In Vitro Synthesis and Structural Characterization of Amorphous Calcium Carbonate. *Z. Anorg. Allg. Chem.* **2005**, *631* (13−14), 2830−2835.
(59) Nassrallah-Aboukaïs, N.; Jacquemin, J.; Decarne, C.; Abi-Aad, E.; Lamonier, J. F.; Aboukaïs, A. Transformation of Vaterite into Calcite in the Absence and the Presence of Copper(II) Species. Thermal Analysis, IR and EPR Study. *J. Therm. Anal. Calorim.* **2003**, *74* (1), 21−27.
(60) Perić, J.; Vučak, M.; Krstulović, R.; Brečević, L.; Kralj, D. Phase Transformation of Calcium Carbonate Polymorphs. *Thermochim. Acta* **1996**, *277* (1−2), 175−186.
(61) Vázquez, G.; Alvarez, E.; Navaza, J. M. Surface Tension of Alcohol + Water from 20 to 50 °C. *J. Chem. Eng. Data* **1995**, *40*, 611−614.

(62) Price, W. S.; Ide, H.; Arata, Y. Solution Dynamics in Aqueous Monohydric Alcohol Systems. *J. Phys. Chem. A* **2003**, *107*, 4784−4789, DOI: 10.1021/jp027257z.
(63) Li, R.; Agostino, C. D.; Mcgregor, J.; Mantle, M. D.; Zeitler, J. A.; Gladden, L. F. Mesoscopic Structuring and Dynamics of Alcohol/Water Solutions Probed by Terahertz Time-Domain Spectroscopy and Pulsed Field Gradient Nuclear Magnetic Resonance. *J. Phys. Chem. B* **2014**, *118*, 10156−10166.
(64) Besagni, G.; Inzoli, F.; De Guido, G.; Pellegrini, L. A. Experimental Investigation on the Influence of Ethanol on Bubble Column Hydrodynamics. *Chem. Eng. Res. Des.* **2016**, *112*, 1−15.
(65) Krishna, R.; Dreher, A.; Urseanu, M.; Rose, by J.; Briggs, A. Influence of Alcohol Addition on Gas Hold-up in Bubble Columns: Development of a Scale Up Model. *Int. Commun. Heat Mass Transfer* **2000**, *27* (4), 465−472, DOI: 10.1016/s0735-1933(00)00129-9.
(66) Xiang, L.; Xiang, Y.; Wen, Y.; Wei, F. Formation of CaCO3 Nanoparticles in the Presence of Terpineol. *Mater. Lett.* **2004**, *58* (6), 959−965.
(67) Fu, L. H.; Dong, Y. Y.; Ma, M. G.; Yue, W.; Sun, S. L.; Sun, R. C. Why to Synthesize Vaterite Polymorph of Calcium Carbonate on the Cellulose Matrix via Sonochemistry Process? *Ultrason Sonochem* **2013**, *20* (5), 1188−1193.
(68) Song, K.; Bang, J. H.; Chae, S. C.; Kim, J.; Lee, S. W. Phase and Morphology of Calcium Carbonate Precipitated by Rapid Mixing in the Absence of Additives. *RSC Adv.* **2022**, *12* (30), 19340−19349.
(69) Oral, Ç. M.; Ercan, B. Influence of PH on Morphology, Size and Polymorph of Room Temperature Synthesized Calcium Carbonate Particles. *Powder Technol.* **2018**, *339*, 781−788.
(70) Rayner-Canham, G.; Overton, T. Charge Densities of Selected Ions. In *Descriptive Inorganic Chemistry*; W. H. Freeman and Company: New York, NY.
(71) Manoli, F.; Dalas, E. Spontaneous Precipitation of Calcium Carbonate in the Presence of Ethanol, Isopropanol and Diethylene Glycol. *J. Cryst. Growth* **2000**, *218* (2), 359−364.
(72) Reichardt, C.; Welton, T.Solvents and Solvent Effects in Organic Chemistry 4th ed.; 2010.
(73) Gebauer, D.; Gunawidjaja, P. N.; Peter Ko, Y.; Bacsik, Z.; Aziz, B.; Liu, L.; Hu, Y.; Bergstrom, L.; Tai, C.-W.; Sham, T.-K.; Eden, M.; Hedin, N. Proto-Calcite and Proto-Vaterite in Amorphous Calcium Carbonates**. *Angew. Chem. Int. Ed.* **2010**, 8889−8891, DOI: 10.1002/anie.201003220.
(74) Qiao, L.; Zizak, I.; Zaslansky, P.; Ma, Y. The Crystallization Process of Vaterite Microdisc Mesocrystals via Proto-Vaterite Amorphous Calcium Carbonate Characterized by Cryo-x-Ray Absorption Spectroscopy. *Crystals* **2020**, *10* (9), 1−12.
(75) Yang, F.; Liu, Y. S.; Feng, X.; Qian, K.; Kao, L. C.; Ha, Y.; Hahn, N. T.; Seguin, T. J.; Tsige, M.; Yang, W.; Zavadil, K. R.; Persson, K. A.; Guo, J. Probing Calcium Solvation by XAS, MD and DFT Calculations. *RSC Adv.* **2020**, *10* (46), 27315.
(76) Kathyola, T. A.; Willneff, E. A.; Willis, C. J.; Dowding, P. J.; Schroeder, S. L. M. Reactive CaCO3 Formation from CO2 and Methanolic Ca(OH)2 Dispersions: Transient Methoxide Salts, Carbonate Esters and Sol-Gels. *ACS Phys. Chem. Au* **2024**, *4*, 555.
(77) Rodriguez-Navarro, C.; Vettori, I.; Ruiz-Agudo, E. Kinetics and Mechanism of Calcium Hydroxide Conversion into Calcium Alkoxides: Implications in Heritage Conservation Using Nanolimes. *Langmuir* **2016**, *32* (20), 5183−5194.
(78) Dickinson, S. R.; McGrath, K. M. Switching between Kinetic and Thermodynamic Control: Calcium Carbonate Growth in the Presence of a Simple Alcohol. *J. Mater. Chem.* **2003**, *13* (4), 928−933.
(79) Harvianto, G. R.; Ahmad, F.; Nhien, L. C.; Lee, M. Vapor Permeation-Distillation Hybrid Processes for Cost-Effective Isopropanol Dehydration: Modeling, Simulation and Optimization. *J. Membr. Sci.* **2016**, *497*, 108−119.
(80) Liew, F. E.; Nogle, R.; Abdalla, T.; Rasor, B. J.; Canter, C.; Jensen, R. O.; Wang, L.; Strutz, J.; Chirania, P.; De Tissera, S.; Mueller, A. P.; Ruan, Z.; Gao, A.; Tran, L.; Engle, N. L.; Bromley, J. C.; Daniell, J.; Conrado, R.; Tschaplinski, T. J.; Giannone, R. J.; Hettich, R. L.; Karim, A. S.; Simpson, S. D.; Brown, S. D.; Leang, C.; Jewett, M. C.; Köpke, M. Carbon-Negative Production of Acetone and Isopropanol by Gas Fermentation at Industrial Pilot Scale. *Nat. Biotechnol.* **2022**, *40* (3), 335−344.

https://doi.org/10.1021/acssuschemeng.5c01554
ACS Sustainable Chem. Eng. 2025, 13, 7549−7561